Applied Catalysis B: Environmental 99 (2010) 336–342

Contents lists available at ScienceDirect

Applied Catalysis B: Environmental

journal homepage: www.elsevier.com/locate/apcatb

Ideal Pt loading for a Pt/CeO_2-based catalyst stabilized by a Pt–O–Ce bond

Miho Hatanaka[a,*], Naoki Takahashi[a], Toshitaka Tanabe[a], Yasutaka Nagai[a], Kazuhiko Dohmae[a], Yuki Aoki[b], Takeru Yoshida[b,1], Hirofumi Shinjoh[a]

[a] Toyota Central R&D Labs., Inc., Nagakute, Aichi 480-1192, Japan
[b] Toyota Motor Corp., Toyota, Aichi 471-8571, Japan

ARTICLE INFO

Article history:
Received 28 April 2010
Received in revised form 22 June 2010
Accepted 6 July 2010
Available online 13 July 2010

Keywords:
Platinum
Ceria
Automotive catalyst
Support interaction
Simulation

ABSTRACT

Pt–O–Ce bond formation under suitable oxidative conditions on the surface of a catalyst support inhibits Pt particle sintering and promotes the redispersion of agglomerated Pt particles. In the present study the influence of Pt loading on changes in the catalytic activity and Pt particle size was evaluated for aged and regenerated Pt/CeO_2-based catalysts. Catalysts with a lower Pt loading exhibited less catalytic deactivation and Pt sintering. There was an ideal Pt loading for which regeneration restored the Pt particle size and the catalytic activity to the same values as for the fresh state. This ideal Pt loading is discussed in terms of Pt anchor sites by considering the structure and composition around Pt on a CeO_2-based catalyst.

1. Introduction

Automotive exhausts equipped with three-way catalysts (TWCs) are now widely used in gasoline-fueled vehicles to meet stringent regulations for carbon monoxide, nitrogen oxides (NO_x) and hydrocarbon (HC) emissions [1]. The main components in TWCs are a precious metal such as palladium, platinum or rhodium as the active catalyst, an inorganic oxide such as γ-alumina (Al_2O_3) or zirconia (ZrO_2) as the support, and an oxygen storage material such as ceria–zirconia (CeO_2–ZrO_2) to maintain stoichiometry at the catalyst surface and achieve higher purification activity [2–4]. Because of the scarcity of natural resources and the increasing price of precious metals, there is a focus on improving the durability of TWCs and applying new insights to develop advanced TWCs with lower precious metal content [5–14].

In principle, when the particle size of a precious metal increases due to agglomeration during the lifetime of a catalyst, the TWC activity deteriorates [15]. Sintering of precious metal particles has been widely investigated, with some researchers focusing on preventing agglomeration on aging [2,16–29]. This issue of TWC deactivation has long been studied in the hydrocarbon reforming industry. Redispersion of agglomerated Pt under certain oxidative heated conditions with chlorine (Cl) has been utilized to reverse the effects of sintering and regenerate spent Pt/Al_2O_3-based reforming catalysts [30–34]. It has been reviled that this treatment at 800–900 K can effectively redisperse Pt agglomerates, however, further several oxidative/reductive treatment returns Pt to sintering, and higher oxidation temperature such as 1000 K leads to drastic sintering of dispersed Pt, because Cl was lost from the catalyst [33]. TWC is exposed to ca. 1000 K and above high temperature exhaust gases from gasoline engines during operation, and the exhaust gas itself fluctuates quickly and dramatically between oxidative and reductive compositions [27]. Obviously, the conventional approach applied to redisperse agglomerated Pt of reforming catalysts is unsuitable for stabilizing or on-board redispersing Pt of TWCs. CeO_2-based inorganic oxides are good supports for stabilizing Pt particles against agglomeration, whereas Pt easily agglomerates on Al_2O_3 under an oxidative atmosphere [2,26–29]. Therefore, use of an appropriate Pt–support interaction is a promising approach for the development of a highly durable TWC.

We found that Pt–O–Ce bond formation under oxidative high-temperature conditions acts as the driving force in preventing sintering [27] and promoting redispersion [35,36] of Pt particles on a CeO_2-based support using X-ray absorption fine structure (XAFS) methodology. We also systematically evaluated changes in Pt oxidation states and nanostructure on a CeO_2-based oxide support after oxidative and reductive treatments [37]. X-ray photoelectron spectroscopy (XPS) revealed that Pt in the oxidized catalyst was in a higher oxidation state than metallic Pt. Spherical aberration-corrected scanning transmission electron microscopy (C_s-corrected STEM) analysis revealed that Pt was dispersed as a

* Corresponding author at: 41-1 Yokomichi, Nagakute, Nagakute-cho, Aichi-gun, Aichi 480-1192, Japan. Tel.: +81 561 717660; fax: +81 561 636150.
E-mail address: e4602@mosk.tytlabs.co.jp (M. Hatanaka).
[1] Present address: Toyota Motor Engineering & Manufacturing North America, 1555 Woodridge Ave, Ann Arbor, MI 48105-9748, USA.

0926-3373/$ – see front matter © 2010 Elsevier B.V. All rights reserved.
doi:10.1016/j.apcatb.2010.07.003

monolayer on the surface of the CeO_2-based support. These results provide evidence of Pt–O–Ce bond formation on the surface of the CeO_2-based oxide support, but not in the bulk, under oxidative conditions.

It is expected that there is an upper limit for the Pt loading at which Pt atoms are stabilized by Pt–O–Ce bonds because the amount of Ce on the support surface is finite. Estimation of this ideal Pt loading is essential for efficient Pt utilization. In the present study, we qualitatively assessed the ideal Pt loading using two approaches. In the first, the influence of Pt loading on the catalytic activity and Pt particle size was determined. In the second, the number of Pt anchor sites was qualitatively predicted based on the structure and composition around Pt on a CeO_2-based catalyst.

2. Experimental

2.1. Support and catalyst preparation

The support consisted of CeO_2, ZrO_2, La_2O_3 and Pr_6O_{11}, denoted as CZLP. The concentration of Ce, Zr, La and Pr cations was 55.0, 36.1, 3.0 and 5.9 mol%, respectively. The support was prepared by dissolving certain amounts of $Ce(NO_3)_3{\cdot}6H_2O$, $ZrO(NO_3)_2{\cdot}2H_2O$, $La(NO_3)_3{\cdot}6H_2O$ (Wako Pure Chemicals) and $Pr(NO_3)_3{\cdot}6H_2O$ (Kojundo Chemical Laboratory) in ion-exchanged water, after which ammonia solution was added. The precipitated material was dried at 673 K for 5 h, calcined at 873 K for 5 h and finally fired at 1323 K for 5 h in air in an Advantec KM-420 muffle furnace to prevent a decrease in specific surface area (SSA) during subsequent aging treatments.

Pt/CZLP catalysts were prepared by conventional wet impregnation of the support powder with $Pt(NH_3)_2(NO_2)_2$ nitric acid solution (Tanaka Kikinzoku Kogyo K.K.). The Pt loading on the catalysts was controlled at 0.10, 0.25, 0.50 and 1.00 g per 100 g of the support, which are denoted as Pt(0.1)/CZLP, Pt(0.25)/CZLP, Pt(0.5)/CZLP or Pt(1)/CZLP, respectively. The Pt-impregnated powders were dried at 393 K overnight and calcined at 773 K for 3 h in a muffle furnace. Then the powders were pressed into disks, crushed and sieved to yield particles of 0.5–1.0 mm in diameter. These samples are referred to as prepared catalysts.

2.2. Catalyst treatments and activity test

Samples of 1 g of the prepared catalysts were placed in the reaction tube of a Best Instruments CATA-5000 system, a conventional fixed flow type reaction apparatus to evaluate the automotive three-way activity. Prior to reaction tests, the catalysts were activated by heating from room temperature to 773 K under a flow of a net stoichiometric fluctuating oxidative and reductive simulated exhaust gas (7000 ml/min) over a period of 10 min and maintained under these conditions for 10 min. The oxidative and reductive simulated gases for pretreatment comprised 0.7% CO/1.12% O_2/0.12% NO/0.05% C_3H_6/10% CO_2/5% H_2O in N_2 and 1.82% CO/0.65% O_2/0.12% NO/0.05% C_3H_6/10% CO_2/5% H_2O in N_2, respectively; the composition was altered every 1 s. Samples after this pretreatment are referred to as fresh catalysts. The fresh catalysts were cooled to 373 K and then heated to 773 K under the same flow as for pretreatment at a rate of 12 K/min. The HC, CO and NO_x concentrations in the outlet gas during the heating process were quantified by a flame ionization HC analyzer, a nondispersive infrared CO analyzer and chemiluminescence NO_x analyzer in a Best Instruments Bex-5900C system.

Samples of 3 g of the prepared catalysts were heated from room temperature to 1223 K under a flow of a net stoichiometric fluctuating oxidative and reductive simulated exhaust gas (500 ml/min) over a period of 1 h and maintained under these conditions for 5 h, then cooled to room temperature in a flow of the same simulated gas. The oxidative and reductive gases for aging consisted of 5% O_2/10% CO_2/3% H_2O in N_2 and 5% CO/10% CO_2/3% H_2O in N_2, respectively; the gases were alternated every 5 min. A 1-g sample after aging was then pretreated in the same manner as for the fresh catalyst. These samples following pretreatment are referred to as aged catalysts. The automotive catalytic activity of the aged catalysts was evaluated using the same procedure as for fresh catalysts.

In our previous study [37], air treatment at 1073 K caused Pt–O–Ce bond formation for the most of 1.5 wt.% Pt loaded on 89 wt.% CeO_2–Al_2O_3 support. Thus, in the present study, samples of 1.5 g following the aging treatments were heated from room temperature to 1073 K under a flow of air (1000 ml/min) over a period of 1 h and maintained under these conditions for 30 min, then cooled to room temperature under an air flow to redisperse agglomerated Pt. Samples (1 g) after the oxidizing treatment were pretreated in the same manner as for the fresh catalyst, except that they were exposed to a net reducing simulated exhaust gas fluctuating between oxidative and reductive conditions to change oxidized Pt to the metallic state to restore the catalytic activity. The oxidative and reductive gases comprised 1.5% CO/1.15% O_2/0.12% NO/0.06% C_3H_6/10% CO_2/5% H_2O in N_2 and 2.62% CO/0.41% O_2/0.12% NO/0.06% C_3H_6/10% CO_2/5% H_2O in N_2, respectively, and were altered every 1 s. These samples following pretreatment are referred to as regenerated catalysts. The activity of the regenerated catalysts was evaluated in the same procedure as for the fresh catalysts.

2.3. CZLP support and Pt/CZLP catalyst characterization

The structure and lattice constant of the CZLP support were evaluated using powder X-ray diffraction (XRD) on a Rigaku RINT 1500-V instrument with Cu K_α radiation ($\lambda = 0.1541$ nm) operated at 40 kV and 350 mA. Data were recorded in the 2θ range from 25° to 85° with an angular step size of 0.01° and an angular scan speed of 0.03°/s. The SSA of the CZLP support was determined by the BET one-point method using a Microdata Microsorp 4232II instrument. CZLP was pretreated under a flow of N_2 (25 ml/min) at 473 K for 20 min and then the gas flow was switched to 30% N_2 in He (25 ml/min) and cooled to 77 K using liquid N_2. The SSA was calculated from the amount of N_2 adsorbed. The primary particle shape of the CZLP support was observed under a Hitachi HF-2000 transmission electron microscope (TEM). CZLP was pulverized using an agate mortar, sonicated in ethanol and deposited on lacey carbon on copper grids for analysis. TEM images were captured using the bright field mode.

The Pt particle diameter of fresh, aged and regenerated Pt/CZLP catalysts after activity tests was quantified using the CO pulse adsorption method on an Ohkura Riken low-temperature CO adsorption apparatus [27,37]. Our previous study [38] revealed that the following experimental procedure is a simple, useful and reliable technique to estimate the Pt particle size in a Pt/CeO_2-based catalyst, because the size of Pt particles determined by this methodology completely showed good agreement with that by XRD and low energy ion scattering (LEIS). A sample of 0.02 g of the catalyst was placed in a sample cell and pretreated according to the procedure established by the Catalysis Society of Japan. First, the catalyst was heated to 673 K in a flow of pure O_2 (20 ml/min) and maintained under the same conditions for 15 min, then the gas flow was changed to 20 ml/min pure He for 10 min, followed by 20 ml/min pure H_2 for 15 min to convert PtO_x into metallic Pt. Finally, the gas flow was changed back to 20 ml/min pure He for 10 min. The catalyst was then cooled to 195 K under a pure He flow using a dry ice/ethanol refrigerant to prevent CO adsorption on the CZLP supports. Then CO (0.75 μmol/pulse) was injected into the catalyst under the He flow until the CO content in the outlet gas reached a

Table 1
Number of atomic layers, Ce and O atoms for CeO_2 support model.

Oriented plane index	(0 0 1)	(0 1 1)	(1 1 1)
Atomic layers	12	8	12
Ce atoms	12	16	16
O atoms	24	32	32

constant value. The amount of CO adsorbed was calculated as the difference between the total amount injected and the sum of all CO detected in the outlet gas. The Pt particle diameter was estimated assuming that one CO molecule adsorbed onto each Pt atom on the surface of hemispherical Pt particles [37,39].

2.4. Pt/CeO_2 geometry optimization

An optimized structure model of a Pt atom on the surface of the CeO_2 support was calculated according to density functional theory (DFT) using the commercial software package DMol^3 in Materials Studio (ver.4.3, Accelrys Inc.). In the present study, the double numerical with polarization (DNP) basis set was adopted as the basis function, and generalized gradient approximation (GGA) in terms of the Perdew-Wang91 functional (PW91) was used to optimize geometries. A CeO_2 unit cell of the fluorite structure was geometrically optimized for the density functional semicore pseudopotential (DSPP) or the all-electron (AER) calculation with fine grade. The lattice constant error for DSPP was +1.30%, whereas that for AER was +2.43%. The optimized CeO_2 unit cell with DSPP was thus used for further simulation. Oxygen-terminated model CeO_2 supports with (0 0 1), (0 1 1) and (1 1 1) surfaces were constructed from the optimized CeO_2 unit cell. The number of atomic layers and Ce and O atoms for (0 0 1)-, (0 1 1)- and (1 1 1)-oriented CeO_2 structure models are summarized in Table 1. The slab model was repeated periodically with a 3-nm vacuum region between the slabs. One Pt atom was placed in the vacuum region at ~0.3 nm from the top surface of each CeO_2 plane. Geometry optimization simulations were carried out for Pt/CeO_2(0 0 1), Pt/CeO_2(0 1 1) and Pt/CeO_2(1 1 1) including surface optimization of the CeO_2 support using fine grade DSPP.

3. Results and discussion

3.1. Changes in TWC activity

Fig. 1 shows the HC, CO and NO_x conversion efficiencies for the fresh Pt(0.1)/CZLP catalyst as a function of the reaction temperature. The CO removal reaction started from ~375 K, whereas HC and NO_x removal reactions started simultaneously at ~450 K. All the conversion efficiencies increased with the reaction temperature

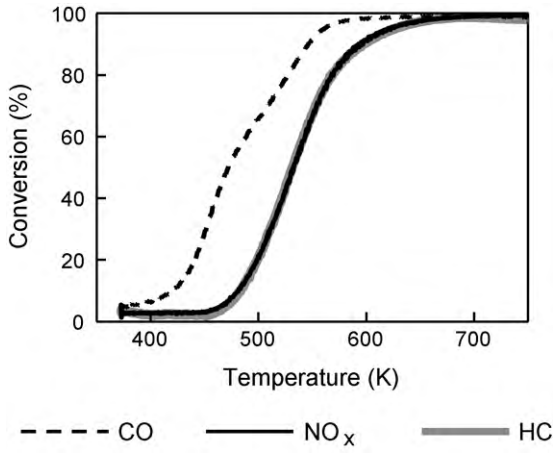

Fig. 1. Automotive three-way catalytic conversion profile for the fresh Pt(0.1)/CZLP catalyst at the net stoichiometric point.

and finally reached 100%. The activity of the Pt/CZLP catalysts was evaluated as the temperature at which 50% of the HC, CO and NO_x in the inlet were removed, denoted as HC-T50, CO-T50 and NO_x-T50, respectively. The HC-T50, CO-T50 and NO_x-T50 values for fresh, aged and regenerated Pt/CZLP catalysts are summarized in Fig. 2a–c as a function of Pt loading. All values for fresh, aged and regenerated Pt/CZLP catalysts monotonically decreased with increasing Pt loading (0.1–1 g/100 g support), indicating that TWC activities strongly depend on the Pt loading and improve for higher Pt loading. The difference in HC-T50 between aged Pt(0.1)/CZY and Pt(1)/CZLP catalysts was 16 K, which is approximately 20% of the difference for the corresponding fresh catalysts (76 K), indicating that the effect of Pt loading in promoting catalytic activity drastically decreased after aging. The difference in HC-T50 between regenerated Pt(0.1)/CZLP and Pt(1)/CZLP catalysts was 31 K, revealing that the positive effect of Pt loading on TWC activity was partially restored by regeneration. Similar trends were observed for both CO-T50 and NO_x-T50. Thus, we focus on HC-T50 to discuss changes in TWC activity for Pt/CZLP catalysts after the different treatments.

To elucidate the influence of Pt loading on the degradation and recovery of TWC activity after aging and regeneration treatments, we calculated the differential HC-T50 between fresh and aged or regenerated catalysts as:

$$\Delta\text{HC-T50}_{\text{aged}} = \text{HC-T50}_{\text{fresh}} - \text{HC-T50}_{\text{aged}} \quad (1)$$

$$\Delta\text{HC-T50}_{\text{regenerated}} = \text{HC-T50}_{\text{fresh}} - \text{HC-T50}_{\text{regenerated}} \quad (2)$$

A smaller absolute value of ΔHC-T50$_{\text{aged}}$ in the negative region indicates that the degradation of TWC activity during aging was

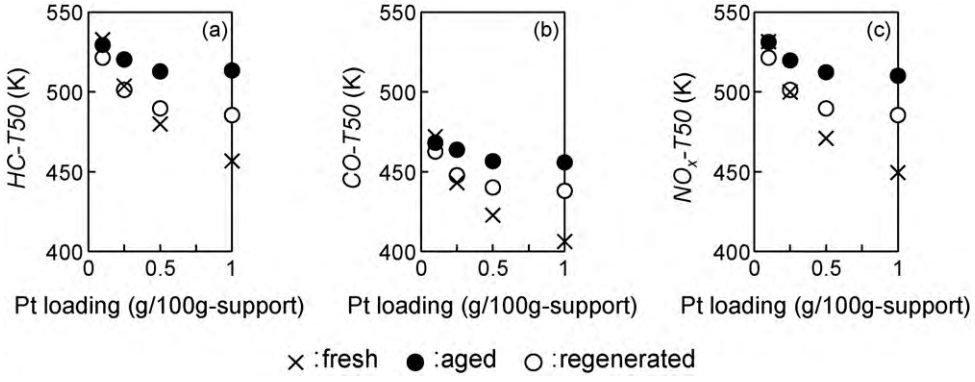

Fig. 2. (a) HC-T50, (b) CO-T50 and (c) NO_x-T50 for fresh, aged and regenerated Pt/CZLP catalysts as a function of Pt loading.

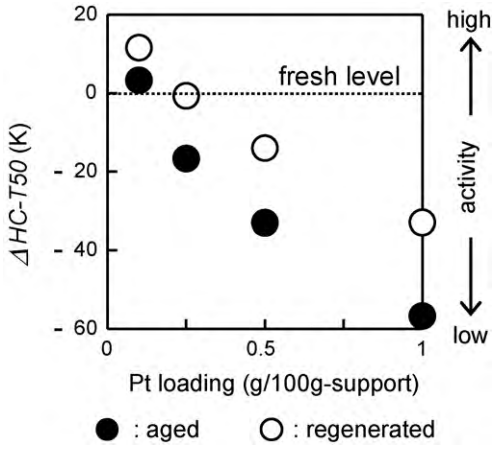

Fig. 3. HC-T50 differential (ΔHC-T50) between fresh and aged or regenerated Pt/CZLP catalysts as a function of Pt loading.

inhibited, whereas a smaller absolute value of ΔHC-T50$_{regenerated}$ in the negative region means that recovery of TWC activity during regeneration was promoted. Both ΔHC-T50$_{aged}$ and ΔHC-T50$_{regenerated}$ are plotted as a function of Pt loading in Fig. 3. It is evident that catalysts with a lower Pt loading have lower absolute ΔHC-T50$_{aged}$ values, with a value of approximately zero for Pt(0.1)/CZLP. The absolute values of ΔHC-T50$_{regenerated}$ were less than the corresponding ΔHC-T50$_{aged}$ for Pt(0.25), Pt(0.5) and Pt(1)/CZLP catalysts, indicating that regeneration of TWC activity is possible, at least in part, by treating the aged catalysts treated under air at 1073 K for 30 min. Similar to ΔHC-T50$_{aged}$, a lower Pt loading leads to a smaller absolute value for ΔHC-T50$_{regenerated}$, indicating that the degree of regeneration of catalytic activity for aged catalysts strongly depends on the Pt loading and is promoted for lower Pt loadings. It is notable that the activity of Pt(0.25)/CZLP was completely recovered to the level for the fresh catalyst, whereas the activity of Pt(0.5) and Pt(1)/CZPL could not be completely restored, indicating that 0.25 g of Pt on 100 g of CZLP is the upper limit for the Pt loading for catalysis in the present study. Catalysts with a Pt loading below this upper limit did not deteriorate, as shown for Pt(0.1)/CZLP in Fig. 3.

3.2. Changes in Pt particle size

The Pt particle diameter (d) for fresh, aged and regenerated Pt/CZLP catalysts as deduced from CO adsorption is shown in Fig. 4.

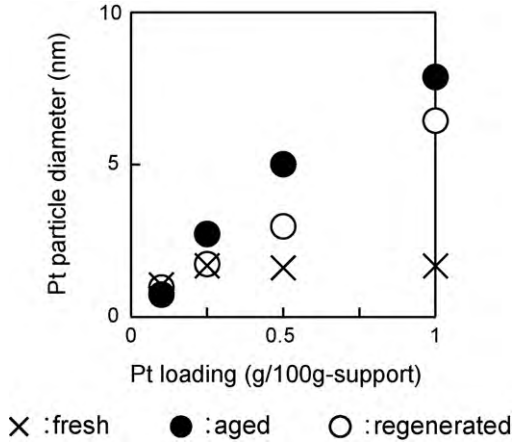

Fig. 4. Pt particle diameter deduced from CO adsorption for fresh, aged and regenerated Pt/CZLP catalysts as a function of Pt loading.

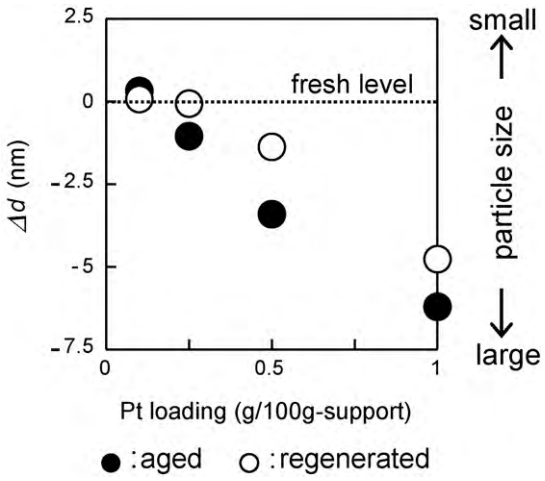

Fig. 5. Pt particle diameter differential (Δd) between fresh and aged or regenerated Pt/CZLP catalysts as a function of Pt loading.

d_{fresh} was almost the same (1–1.6 nm) even when the Pt loading was increased by a factor of 10 (0.1–1 g/100 g support), indicating that the Pt particle size was hardly dependent on the Pt loading for fresh catalysts, whereas d_{aged} and $d_{regenerated}$ increased monotonically with Pt loading. To elucidate the influence of Pt loading on sintering and redispersion of Pt particles after aging or regeneration treatment, we calculated the differential particle diameter between fresh and aged or regenerated catalysts as:

$$\Delta d_{aged} = d_{fresh} - d_{aged} \quad (3)$$

$$\Delta d_{regenerated} = d_{fresh} - d_{regenerated} \quad (4)$$

A smaller absolute value of Δd_{aged} in the negative region indicates that Pt sintering in the aged catalyst was inhibited, whereas a smaller absolute value of $\Delta d_{regenerated}$ in the negative region means that Pt redispersion in the regenerated catalyst was promoted. Fig. 5 shows Δd_{aged} and $\Delta d_{regenerated}$ as a function of Pt loading. Catalysts with a lower Pt loading had a lower absolute value of Δd_{aged}, with $\Delta d_{aged} \approx 0$ for Pt(0.1)/CZLP. The absolute $\Delta d_{regenerated}$ value for Pt(0.25), Pt(0.5) and Pt(1)/CZLP catalysts was less than the corresponding Δd_{aged} value, indicating that redispersion of agglomerated Pt particles in these catalysts is possible, at least in part, by treatment under air at 1073 K for 30 min. Similar to Δd_{aged}, a lower Pt loading led to a smaller absolute value for $\Delta d_{regenerated}$, indicating that the degree of redispersion of agglomerated Pt in the aged catalysts strongly depends on the Pt loading and is promoted at lower Pt loading. It is notable that agglomerated Pt in Pt(0.25)/CZLP was redispersed to a degree similar to the fresh catalyst, whereas Pt particles in Pt(0.5) and Pt(1)/CZPL could not redispersed to the fresh levels, indicating that 0.25 g of Pt on 100 g of CZLP is the upper Pt loading to restore Pt dispersion in the present study. Catalysts with a Pt loading below this upper limit did not exhibit agglomeration, as shown for Pt(0.1)/CZLP in Fig. 5.

3.3. Relation between catalytic activity and number of active sites

Our previous research into the Pt oxidation state and nanostructure on a CeO_2-based oxide support revealed that metallic Pt particles of 1–2 nm in diameter under reductive conditions are reversibly changed to a monolayer of Pt in a higher oxidation state than metallic Pt that forms a complex with Ce on the support surface under oxidative conditions [37]. Operational experiments in which simultaneous measurement of the state of catalytic active sites and catalytic performance of a Pt/Al_2O_3 catalyst revealed that metallic Pt sites are the active sites for catalytic reactions under

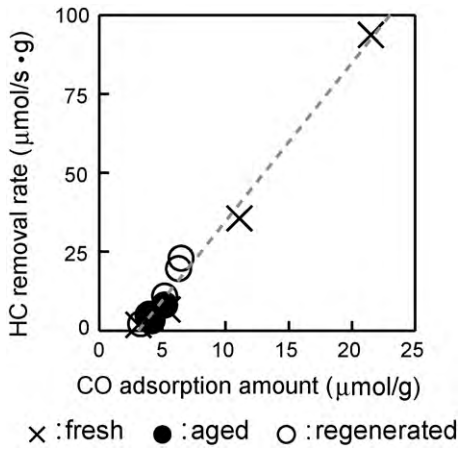

Fig. 6. HC removal rate at 500 K versus CO adsorption for fresh, aged and regenerated Pt/CZLP catalysts.

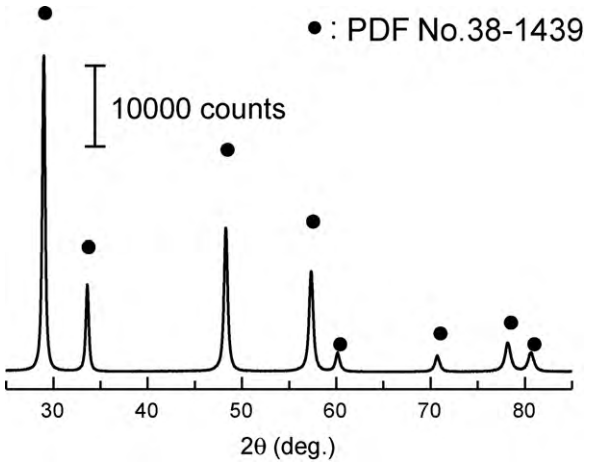

Fig. 7. XRD pattern of the CZLP support calcined at 1323 K.

both net oxidative and reductive conditions [40]. Metallic Pt sites on the surface of Pt particles can be quantified by CO pulse adsorption. Thus, as Anderson et al. reported in their studies on reforming catalyst [33,34], the catalytic activity of the Pt/CZLP catalysts should be proportional the amount of CO adsorbed, if there is no large difference in active site quality among catalysts with different Pt loadings. The HC removal rate at 500 K was deduced from extrapolation of the Arrhenius plot of HC conversion between 10% and 20% conversion efficiency for each catalyst. The HC removal rate plotted as a function of CO adsorption for each catalyst in Fig. 6 yields a linear relationship with negative *y*-intercept (positive *x*-intercept). The good linearity suggests that TWC activity in the present study is dominated by the number of active sites on the surface of Pt particles and the quality of the active sites is hardly affected by the Pt loading or aging or regeneration treatment. We think that the negative *y*-intercept was caused by differences in the pretreatment conditions between catalytic activity tests and CO pulse adsorption experiments. Some of the supported Pt, which can be reduced to the metallic state during the CO adsorption pretreatment (100% H_2 at 673K for 15 min), can probably not be reduced to the metallic state during the pretreatment for catalytic reaction tests (net stoichiometric or reductive conditions at 773K for 15 min). A result supporting this notion was obtained in our previous study: approximately 35% of the surface Pt existed in an oxidizing state on a CeO_2-based oxide support even when treated with 3% H_2 at 873 K for 1 h [37]. Further investigations are required to confirm this.

3.4. Ideal Pt loading

The results in Sections 3.1 and 3.2 indicate that there is the upper Pt loading (0.25 g Pt/100 g CZLP) for both the catalytic activity and the Pt particle size. When the Pt loading approached this value, the catalytic activity and Pt particle size were restored to similar level as in the fresh state as a result of Pt–support interaction. In the following, we discuss this upper limit from the viewpoint of Pt anchor sites by considering the structure and composition around Pt on the CeO_2-based catalyst. The structure and composition were evaluated by geometry optimization simulation and probabilistic estimation on the surface of the fluorite-type CeO_2 support, respectively.

Our previous studies revealed that Pt–O–Ce bonds are formed on the surface of the CeO_2-based support, but not in the bulk [27,37]. Thus, the ideal Pt loading in terms of the mass of Pt per 100 g of the CZLP support (X) can be written as:

$$X = \frac{(S \times 100)}{s} \times \frac{\delta}{100} \times \frac{M_{Pt}}{N_A} \quad (5)$$

where S (m^2/g), s (m^2), δ (%), M_{Pt} (g/mol) and N_A (mol^{-1}) are the support SSA, the area occupied by one Pt atom, the probability that each site is a Pt anchor site, the atomic weight of Pt and the Avogadro constant, respectively. For the CZLP support, $S = 24.9\ m^2/g$, $M_{Pt} = 195.1$ g/mol and $N_A = 6.02 \times 10^{23}\ mol^{-1}$. Thus, X can be computed when s and δ are fixed.

Fig. 7 shows the XRD pattern of the CZLP support calcined at 1323 K. Comparison of this pattern with PDF#38-1439 ($Ce_{0.4}Zr_{0.6}O_2$) reveals that the CZLP support has a fluorite-type structure. Ichikawa et al. reported that the surface of small CeO_2 particles comprised (0 0 1) and (0 1 1) planes, whereas (1 1 1) dominated in large CeO_2 particles [41]. TEM images captured by Pozdnyakova et al. revealed that surface of CeO_2 particles of <10 nm was oriented with (0 0 1), (0 1 1) and (1 1 1) planes [42]. The size of the primary CZLP particles in Fig. 8 is approximately 10 nm. Thus it is reasonable to assume that the primary CZLP particles are composed of (0 0 1), (0 1 1) and (1 1 1) planes. If exposure ratio of (0 0 1), (0 1 1) and (1 1 1) planes at the surface of CZLP particles are proportional to surface energies ratio derived from DFT simulation, it is expected to be 1.5×10^{-17}, 12.7 and 87.3, predicting that CZLP

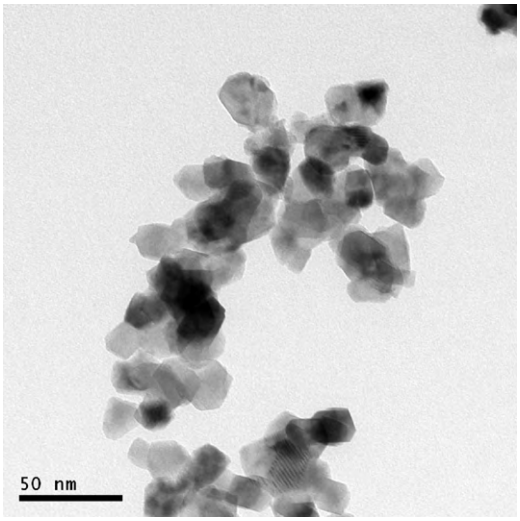

Fig. 8. TEM image of the primary particles of the CZLP support.

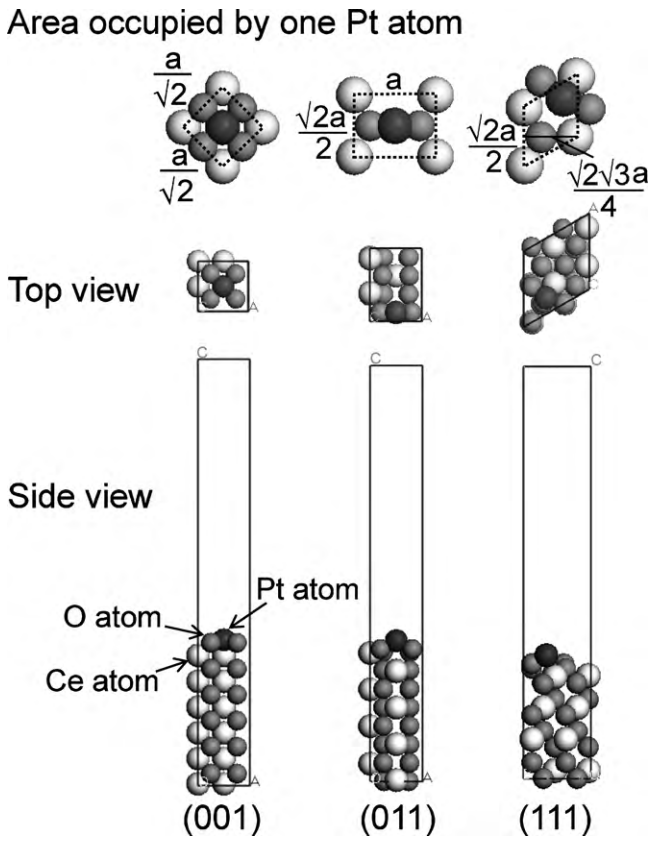

Fig. 9. Top and side views of the optimized structure and area occupied by one Pt atom on CeO_2 (0 0 1), (0 1 1) and (1 1 1) planes.

surface is dominantly composed of (1 1 1) planes. If this assumption could be adopted, the shape of individual primary particles must be principally octahedral crystal. However, as shown in Fig. 8, any primary particle of the CZLP support does not have such a specific shape. More over, our previous *Cs*-STEM image captured that (0 0 1) plane obviously exists at the surface of CeO_2-based support [37], whereas this plane is hardly expected to be exposed from DFT simulation. The discrepancy between simulation and experimental results should be caused from that DFT assumed boundless, flat and homogeneous planes whereas employed actual primary support is composed of nanoparticles. Mardier et al. presumed that the surface of a CeO_2 support was equally composed of (0 0 1), (0 1 1) and (1 1 1) planes to estimate the number of surface oxygen atoms for CeO_2 and CeO_2–ZrO_2 in their study on oxygen storage and release capacity [43]. Thus, it is reasonable to assume that the surface of primary CZLP particles is equally composed of (0 0 1), (0 1 1) and (1 1 1) planes. Fig. 9 shows top and side views of the optimized structures for Pt atoms on CeO_2 (0 0 1), (0 1 1) and (1 1 1) planes as simulated in Section 2.4. The area occupied by one Pt atom on each plane can be defined as:

$$S_{(0\,0\,1)} = \left(\frac{a}{\sqrt{2}} \times 10^{-9}\right)^2 \tag{6}$$

$$S_{(0\,1\,1)} = \left(\frac{\sqrt{2}a}{2} \times 10^{-9}\right) \times (a \times 10^{-9}) \tag{7}$$

$$S_{(1\,1\,1)} = \frac{\sqrt{2}a}{2} \times 10^{-9} \times \left(\frac{\sqrt{2}\sqrt{3}a}{4} \times 10^{-9}\right) \tag{8}$$

where a (m) is the lattice constant of the support, which is 0.533 nm for CZLP according to XRD results. Since we assume that the CZLP surface is composed of (0 0 1), (0 1 1) and (1 1 1) planes in equal

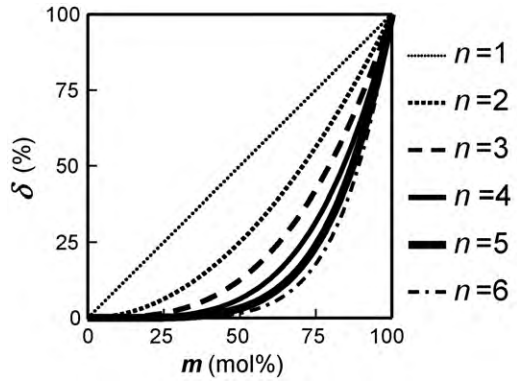

Fig. 10. Pt anchor site probability versus Ce cation concentration in the support.

proportions, the average area occupied by one Pt atom is:

$$S = \frac{(S_{(0\,0\,1)} + S_{(0\,1\,1)} + S_{(1\,1\,1)})}{3} = \left(\frac{a^2}{2} + \frac{\sqrt{2}a^2}{2} + \frac{\sqrt{3}a^2}{4}\right) \times \frac{10^{-18}}{3} \tag{9}$$

Next, the composition around Pt on the support surface is discussed. The assumption that the Pt stabilization force is identical on each of the CeO_2 planes results in the following probability for Pt anchor sites:

$$\delta = \left(\frac{m}{100}\right)^n \times 100 \tag{10}$$

δ is a function of the Ce cation concentration in the of support (m) and the number of Ce atoms that interact with oxidized Pt (n). Fig. 10 shows plots of δ (n = 1,. . .,6) as a function of m. In the present study m is 55.0 mol%, so δ can be calculated when n is defined. Fig. 11 shows plots of the ideal Pt loading (X) as a function of n. The dashed line denotes 0.25 g of Pt/100 g of CZLP, the experimental upper Pt loading for which Pt can be restored to the fresh state (Figs. 3 and 5). Substituting n = 5 leads to a value of X = 0.261 g Pt/100 g CZLP (105 μg Pt/1 m^2 CZLP), which is approximately equivalent to the experimental value for Pt/CZLP. Thus, we can conclude from this computation that 5 Ce atoms on average interact with Pt to form Pt anchor sites. If this hypothesis can be proved, the geometry optimization simulation provides Pt anchor site for (0 0 1), (0 1 1) and (1 1 1) surfaces as shown in Fig. 12. Each Pt anchor site is depicted with one Pt atom and O atoms are in direct contact with Pt and the five nearest-neighbor Ce atoms to Pt. Further study is required to evaluate the reliability of this proposal.

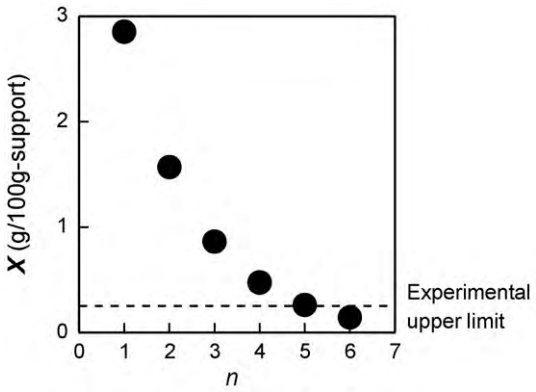

Fig. 11. Ideal Pt loading versus number of Ce atoms interacting with oxidized Pt.

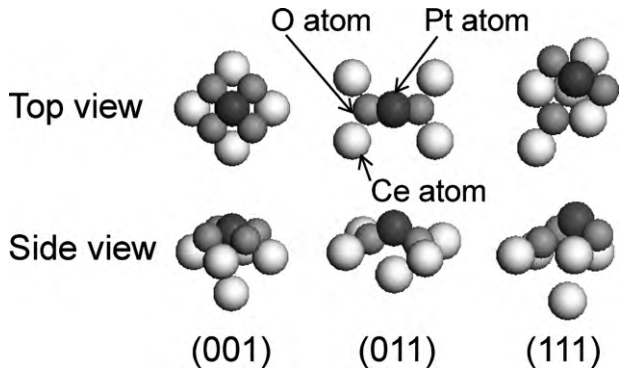

Fig. 12. Predicted Pt anchor site structure at (0 0 1), (0 1 1) and (1 1 1) surfaces.

4. Conclusions

We investigated the ideal Pt loading to stabilize Pt atoms through Pt–O–Ce bond formation. The ideal Pt loading has an upper limit at which both the catalytic activity and Pt particle size of aged catalysts were restored to the same level as for the fresh state on regeneration. This upper limit in the present study was 0.25 g of Pt for 100 g of CZLP support. To estimate the number of Pt anchor sites, an equation was devised based on the structure and composition around Pt on the support. This equation predicted that 5 Ce atoms on average interact with one Pt atom to form a Pt anchor site. Pt loading should be below the upper limit for the ideal amount to achieve good catalytic performance during the catalyst lifetime. The novel insights in the present study have been applied for practical TWCs to reduce their Pt loading [44].

Acknowledgements

We are grateful to Professor Dr. Kazunari Domen of the University of Tokyo for fruitful discussions. We thank Dr. Yasuhiro Ikuta and other colleagues in Toyota Motor Corporation and Toyota Central R&D Labs., Inc. for their help and many suggestions on this work.

References

[1] S. Matsumoto, Catal. Today 90 (2004) 183.
[2] H.C. Yao, Y.F. Yao, J. Catal. 86 (1984) 254.
[3] M. Ozawa, M. Kimura, A. Isogai, J. Alloys Compd. 193 (1993) 73.
[4] Y. Nagai, T. Yamamoto, T. Tanaka, S. Yoshida, T. Nonaka, T. Okamoto, A. Suda, M. Sugiura, Catal. Today 74 (2002) 225.
[5] J.C. Summers, J.J. White, W.B. Williamson, SAE Technical Paper 890794, 1989.
[6] R.J. Brisley, G.R. Chandler, H.R. Jones, P.J. Anderson, P.J. Shady, SAE Technical Paper 950259, 1995.
[7] E. Jobson, O. Hjortsberg, S. L. Anderson, I. Gottberg, SAE Technical Paper 960801, 1996.
[8] M.V. Twigg, N.R. Collins, D. Morris, R.J. Brisley, A.J. Ribeiro, G.D. Borgialli, SAE Technical Paper 2000-01-3303, 2001.
[9] Y. Nishihata, J. Mizuki, T. Akao, H. Tanaka, M. Uenishi, M. Kumura, T. Okamoto, N. Hamada, Nature 411 (2002) 164.
[10] T. Yoshida, A. Sato, H. Suzuki, T. Tanabe, N. Takahashi, SAE Technical Paper 2006-01-1061, 2006.
[11] N.R. Collins, M.V. Twigg, Top. Catal. 42/43 (2007) 323.
[12] S.Y. Christou, A.M. Efstathiou, Top. Catal. 42/43 (2007) 415.
[13] T. Tanabe, Y. Nagai, K. Dohmae, H. Sobukawa, H. Shinjoh, J. Catal. 257 (2008) 117.
[14] D.M. Fernandes, A.A. Neto, M.J.B. Cardoso, F.M.Z. Zotin, Catal. Today 133–135 (2008) 574.
[15] Y. Sakamoto, K. Higuchi, N. Takahashi, K. Yokota, H. Doi, M. Sugiura, Appl. Catal. B 23 (1999) 159.
[16] Y.F. Chu, E. Ruckenstein, J. Catal. 55 (1978) 281.
[17] I. Sushumna, E. Ruckenstein, J. Catal. 109 (1988) 433.
[18] M. Funabiki, T. Yamada, SAE Technical Paper 881684, 1988.
[19] N. Miyoshi, S. Matsumoto, M. Ozawa, M. Kimura, SAE Technical Paper 891970, 1989.
[20] E. Ruckenstein, B. Pulvermacker, J. Catal. 29 (1973) 224.
[21] B.K. Chakraverty, J. Phys. Chem. Solids 28 (1967) 2401.
[22] P. Wynblatt, N.A. Gjoostein, Prog. Solid State Chem. 9 (1975) 21.
[23] P.C. Flynn, S.E. Wanke, J. Catal. 34 (1974) 390.
[24] A. Morikawa, T. Suzuki, T. Kanazawa, K. Kikuta, A. Suda, H. Shinjoh, Appl. Catal. B 78 (2008) 210.
[25] H. Muraki, H. Sobukawa, M. Kimura, A. Isogai, SAE Technical Paper 900610, 1990.
[26] E.C. Su, W.G. Rothschild, J. Catal. 99 (1986) 506.
[27] Y. Nagai, T. Hirabayashi, K. Dohmae, N. Takagi, T. Minami, H. Shinjoh, S. Matsumoto, J. Catal. 242 (2006) 103.
[28] A.F. Diwell, R.R. Rajaram, H.A. Shaw, T.J. Truex, Stud. Surf. Sci. Catal. 71 (1991) 139.
[29] L.L. Murrell, S.J. Tauster, D.R. Anderson, Stud. Surf. Sci. Catal. 71 (1991) 275.
[30] R.M.J. Fiedorow, S.E. Wanke, J. Catal. 43 (1976) 34.
[31] J.B. Peri, J. Catal. 52 (1978) 144.
[32] G.I. Straguzzi, H.R. Aduriz, C.E. Gigola, J. Catal. 66 (1980) 171.
[33] J.A. Anderson, M.G.V. Mordente, C.H. Rochester, J. Chem. Soc., Faraday Trans. 1 85 (1989) 2983.
[34] J.A. Anderson, M.G.V. Mordente, C.H. Rochester, J. Chem. Soc., Faraday Trans. 1 85 (1989) 2991.
[35] Y. Nagai, N. Takagi, Y. Ikeda, K. Dohmae, T. Tanabe, G. Guilera, S. Pascarelli, M. Newton, H. Shinjoh, S. Matsumoto, Stud. Surf. Sci. Catal. 172 (2007) 623.
[36] Y. Nagai, K. Dohmae, Y. Ikeda, N. Takagi, T. Tanabe, N. Hara, G. Guilera, S. Pascarelli, M.A. Newton, O. Kuno, H. Jiang, H. Shinjoh, S. Matsumoto, Angew. Chem. Int. Ed. 47 (2008) 9303.
[37] M. Hatanaka, N. Takahashi, N. Takahashi, T. Tanabe, Y. Nagai, A. Suda, H. Shinjoh, J. Catal. 266 (2009) 182.
[38] T. Tanabe, Y. Nagai, T. Hirabayashi, N. Takagi, K. Dohmae, N. Takahashi, S. Matsumoto, H. Shinjoh, J.N. Kondo, J.C. Schouten, H.H. Brongersma, Appl. Catal. A 370 (2009) 108.
[39] J.A. Anderson, R.A. Daley, S.Y. Christou, A.M. Efstathiou, Appl. Catal. B 64 (2006) 189.
[40] T. Tanabe, Y. Nagai, K. Dohmae, N. Takagi, N. Takahashi, H. Shinjoh, Top. Catal. 52 (2009) 1433.
[41] N. Ichikawa, S. Sato, R. Takahashi, T. Sodesawa, H. Fujita, T. Atoguchi, A. Shiga, J. Catal. 239 (2006) 13.
[42] O. Pozdnyakova, D. Teschner, A. Wootsch, J. Kröhnert, B. Steinhauer, H. Sauer, L. Toth, F.C. Jentoft, A. Knop-Gericke, Z. Paál, R. Schlögl, J. Catal. 237 (2006) 1.
[43] Y. Madier, C. Descorme, A.M. Le Govic, D. Duprez, J. Phys. Chem. B 103 (1999) 10999.
[44] Y. Aoki, T. Yoshida, T. Tanabe, M. Hatanaka, Y. Nagai, S. Sakagami, M. Shimizu SAE Technical Paper 2009-01-1081, 2009.